Physica Scripta. Vol. 41, 537–541, 1990.

Temperature Dependence of the Electronic Structure of Oxides: MgO, $MgAl_2O_4$ and Al_2O_3

M. L. Bortz,* R. H. French,† D. J. Jones, R. V. Kasowski and F. S. Ohuchi

E. I. DuPont de Nemours and Co. Inc., Central Research, Experimental Station, Wilmington DE, 19880, U.S.A.

Received July 16, 1989; in revised form August 11, 1989, accepted November 11, 1989

Abstract

We have studied the room temperature optical reflectivity of MgO, $MgAl_2O_4$, and α-Al_2O_3 from 5 to 40 eV using a novel spectrophotometer with a laser plasma light source. Structure in the imaginary component of the dielectric response is analysed using critical point line shapes, and the origins of the major transitions in MgO and $MgAl_2O_4$ are determined using an *ab initio* pseudofunction band structure calculation of MgO. The exciton reflectivity has been studied in the three materials at temperatures between 300 and 1500 K, and exciton-phonon coupling appears to increase from MgO to α-Al_2O_3. The temperature dependence of the higher lying interband transitions in MgO has been determined to 1100 K, and we find that while the temperature dependence of the onset transitions at Γ and X are nearly identical (-1.22 meV/K at Γ), higher lying transitions have very different temperature dependences. Furthermore with increasing temperature the X point valence band separation increases at a rate of 0.38 meV/K, while the conduction band separation at X decreases at -0.41 meV/K.

1. Introduction

New and demanding applications have generated intense interest in the electronic structure of oxide materials. While the alkali halides have been extensively studied using optical techniques, and covalent semiconductors studied using optical and electron spectroscopies, the more complex oxide materials have not seen such thorough investigations. This is in part due to the passive roles these materials play in traditional technological applications. However, there is increasing interest in MgO and Al_2O_3 as substrate materials for thin film growth, Al_2O_3 and $MgAl_2O_4$ as tunable laser materials, and more complex oxides as nonlinear optical media. Thus a more fundamental understanding of the basic electronic structure of oxide materials is desirable.

The room temperature electronic structure of MgO has been studied previously using optical spectroscopy [1] and band structure methods [2]. Previous optical reflectivity measurements of α-Al_2O_3 [3] have not allowed careful interpretation, and there is no consensus on the fundamental electronic structure of this material. There is very little information available on the more complex oxide $MgAl_2O_4$ spinel. In addition, the effect of temperature on the band states is important in many applications. For example, the processing and applications of these oxide materials all involve elevated temperatures. While the temperature dependence of the electronic structure of semiconductors has been studied [4], only recently have investigations in the VUV begun to uncover the effect of temperature on excitonic and band gap transitions in α-Al_2O_3 [5] and MgO [6]. In this paper we present the room temperature reflectivity and imaginary component of the dielectric response for MgO, $MgAl_2O_4$ and α-Al_2O_3 from 5 to 40 eV. The origins of the major transitions in MgO and $MgAl_2O_4$ are assigned to critical points based on an ab-initio pseudofunction (PSF) band structure calculation [7] of MgO. We then use the exciton line-shape analysis developed by Toyozawa [8] to study the temperature dependence of the Γ point excitons observed at the band gap energy. The temperature dependence of the higher lying interband transitions of MgO has been determined from 300 to 1100 K and is used to identify temperature induced changes in the band structure.

2. Experimental

Reflectivity measurements have been performed at room and elevated temperature from 5 to 40 eV using a Laser Plasma Light Source [9]. A high power, nanosecond pulse from a Nd:YAG laser is focussed onto the surface of a Samarium metal target producing a high intensity pulse of continuum radiation extending from the visible to the soft X-ray region. The plasma light enters a spectrophotometer, which is the subject of another paper [10]. The wavelength resolution is 0.3 nm above and 0.1 nm below 130 nm, and reflectivity magnitudes are reproducible to within $\Delta R/R = 5\%$.

MgO single crystals [11] are cleaved under nitrogen and transferred into the spectrophotometer with minimal exposure to air. Synthetic basal plane α-Al_2O_3 and $MgAl_2O_4$ spinel [12] lack simple cleavage planes and are polished with a 1 μm diamond paste followed by a colloidal silica based chemical polish. Samples are heated with a 10.6 μm, 150 Watt CO_2 laser incident on the sample and temperatures are measured by thermocouples embedded in the sample or optical pyrometry. In some cases the reflectivities are multiplied by a constant to agree with the known refractive index in the visible.

3. Electronic Structure of MgO, $MgAl_2O_4$ and Al_2O_3

The measured reflectivities of single crystal MgO, $MgAl_2O_4$ and α-Al_2O_3 are shown in Fig. 1. The data has not been smoothed. The materials are all transparent in the visible, and the excitonic transition associated with the fundamental absorption edge increases in the series from 7.6 to 9.1 eV. As expected, the predominantly ionic MgO exhibits the strongest structure throughout the VUV. However, the $MgAl_2O_4$ reflectivity is very similar to MgO, showing prominent high energy features at 10.0, 14.3, and 19.0 eV. α-Al_2O_3 displays the broadest reflectivity features, but six high lying features are observed. At photon energies above 25 eV the reflectivity

* Present address, Department of Applied Physics, Stanford University, Stanford, California 93405, U.S.A.

† To whom correspondence should be addressed.

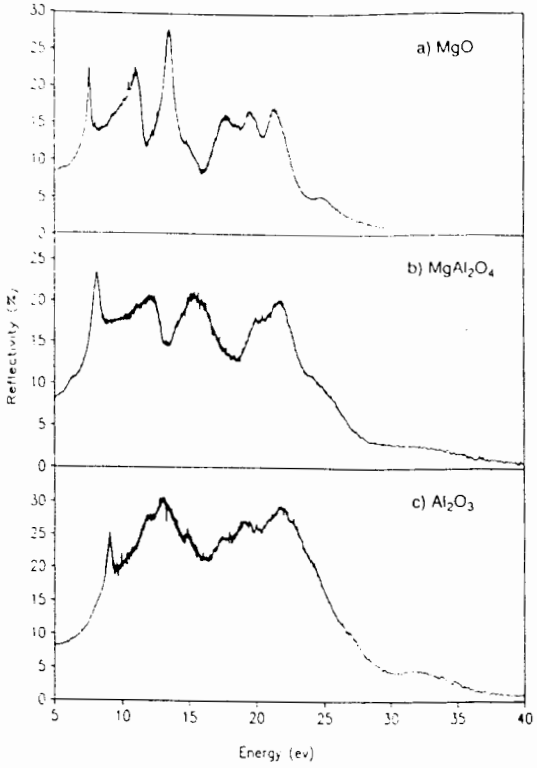

Fig. 1. Reflectivity of (a) MgO, (b) $MgAl_2O_4$, and (c) α-Al_2O_3, obtained using a laser plasma light source.

magnitudes begin to decrease. Except for small features near 32 eV from O 2*s* states, the interband transitions are exhausted and by 40 eV the reflectivity drops to less than 1%. Shown in Fig. 2 are the imaginay components of the dielectric constant ε_2 for the three materials, determined using an FFT based Kramers–Kronig technique [13]. Using semianalytic curve fitting we can identify the critical point structure in ε_2. In all three materials the excitonic and interband onset are nearly

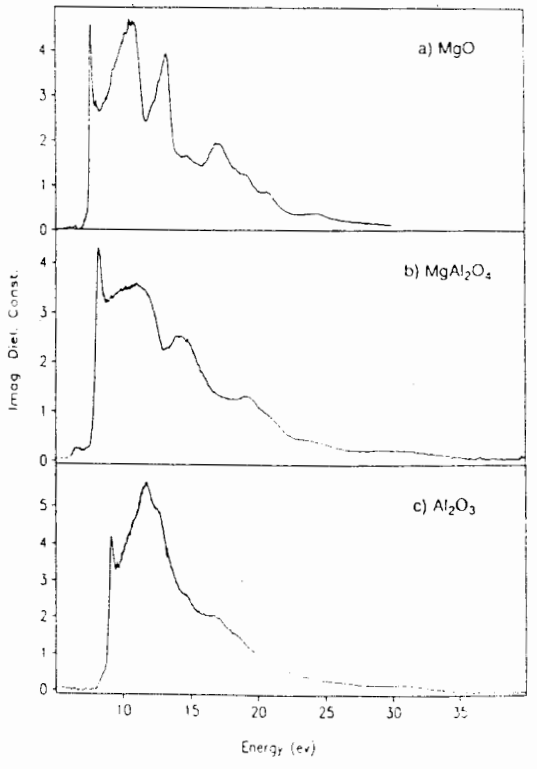

Fig. 2. Imaginary component ε_2 of the dielectric response of (a) MgO, (b) $MgAl_2O_4$ and (c) α-Al_2O_3.

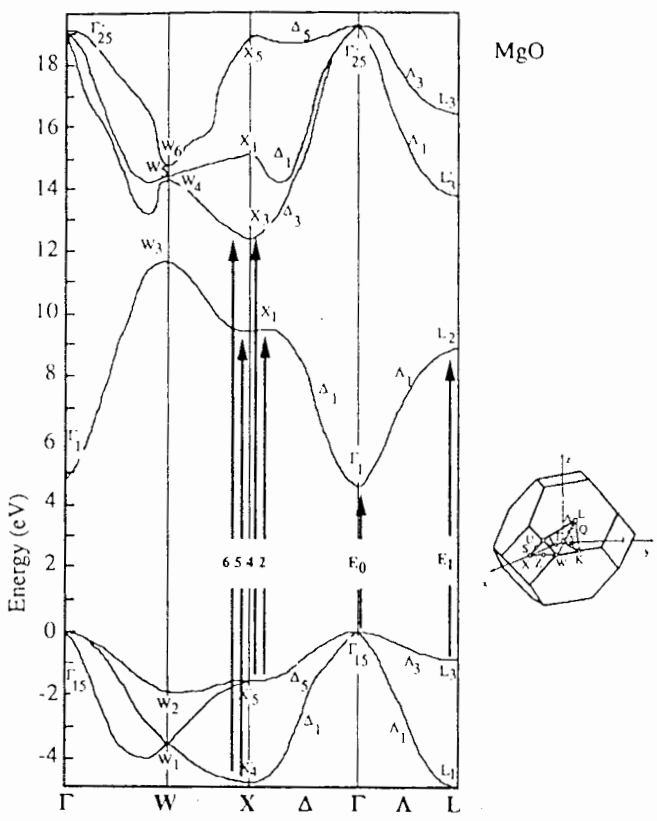

Fig. 3. The band structure of MgO calculated using pseudo function technique.

degenerate, making an exact determination of the fundamental gap difficult.

3.1. *MgO*

The reflectivity and calculated ε_2 of MgO agree very well with previously published results [1]. Shown in Fig. 3 is the PSF band structure of MgO calculated under the local density approximation (LDA). The experimental and calculated interband transition energies for MgO are listed in Table I. The LDA band gap energy of MgO is 4.6 eV, yet we have found the best correspondence between the critical point energies and the LDA band energies using the as calculated band energies. This may arise because the reduced LDA band gap leads to increased hybridization and dispersion of the conduction bands. Clearly, the fundamental absorption is a Γ_{15}–Γ_1 transition, and the increase in ε_2 at 9 eV is due to transitions from L_3 to L_2'. The rest of the higher lying features in ε_2 can be accounted for by transitions either at or near the *X* point. The peak near 10.7 eV is associated with a X_5' to X_1 transition, and the sharp structure at 14 eV arises from the

Table I. *Room temperature critical point energies for MgO*

	E (exp.) (eV)	*E* (theo.) (eV)	Assignment
E_0	7.5 (M_0)	4.6	$\Gamma_{15} \rightarrow \Gamma_1$
E_1	8.7 (M_0)	9.8	$L_3 \rightarrow L_2', \Lambda$
E_2	10.5 (M_1)	11	$X_5' \rightarrow X_1$
E_3	11.0 (M_2)		
E_4	13.2 (M_1)	13.9	$X_5' \rightarrow X_4$
E_5	13.3 (M_2)	14.2	$X_4' \rightarrow X_1 Z$
E_6	16.1 (M_0)	17.1	$X_4' \rightarrow X_1$
E_7	17.4 (M_2)		

near degeneracy of the X_5' to X_3 and X_4' to X_1 transitions. Another significant feature arises from X_4' to X_3 transitions starting at 16.1 eV. The differences in the critical point energies given by E_5-E_2 and E_6-E_4 and their assignments allow us to determine a $X_5'-X_4'$ valence band separation of 2.8 or 2.9 eV respectively, which compares nicely with the calculated separation of 3.2 eV. Similarly, we determine the X_3-X_1 conduction band separation from E_4-E_2 and E_6-E_5 to be 2.7 or 2.8 eV, in agreement with the PSF calculation of 2.9 eV. Although there are other higher lying features their assignment is more difficult due to the possibility of many competing transitions. While the PSF calculation does not predict the band gap accurately, the agreement between the transition energies and band separations at X is very good.

The agreement between the optical data presented here and the previous results of Roessler and Walker is excellent. However, conflicts between the two band structure calculations used to account for the optical data give rise to different transition assignments. There is agreement in the assignment of the fundamental gap and the increase between 9 and 11 eV due to transitions at L. However, the empirical pseudopotential calculation [2] overestimates the X point transition energies relative to our calculation. Thus, Roessler and Walker attribute the increase at 13.2 eV to a $X_5'-X_1$ M_0 point and transitions along the $\Delta_5-\Delta_1$ line, and the decrease at 13.3 eV to the M_2 point formed along the $\Sigma_4-\Sigma_1$ line. They also attribute the increase at 16.1 eV to $X_5'-X_3$ transitions. Our calculation places these transitions at lower energies, and we have used transitions from X_4' to account for the M_2 point at 13.3 eV and the M_0 point at 16.1 eV. While identification of the specific band transitions differs due to conflicts in the calculations, there is good agreement that a majority of the higher lying optical activity is due to band parallelism near X.

3.2. $MgAl_2O_4$

In addition to MgO we have studied the related oxide material $MgAl_2O_4$. This material also has cubic symmetry but a more complex unit cell consisting of tetrahedrally coordinated Mg and octahedrally coordinated Al. The reflectivity and ε_2 are shown in Figs 1(b) and 2(b), respectively. MgO and $MgAl_2O_4$ have very similar features, seen by comparing the optical data. An excitonic transition is followed by a gradual increase in ε_2, followed by a sharp drop, and then another sharp peak. The observed critical points are tabulated in Table II. We have not yet calculated the band structure of $MgAl_2O_4$, but we can assume similar assignments for the two materials, in which the optical activity is due in large part to transitions at X. Using the energies from Table II, we derive conduction band separations analogous to a X_3-X_1 separation of 3.2 ± 0.2 eV, and a valence band separation analogous to a $X_5'-X_4'$ separation of 3.9 ± 0.2 eV. The increase in valence band X point separation is appealing since $MgAl_2O_4$ is more covalent than MgO, and using high resolution valence band X-ray Photoelectron Spectroscopy we measure a valence band width increase from 7.5 eV in MgO to 8.1 eV in $MgAl_2O_4$. Furthermore the valence band peak separation increases from 2.6 eV in MgO to 4.1 eV in $MgAl_2O_4$ in very good agreement with the optically determined X point valence band separation. Thus, the electronic structure of $MgAl_2O_4$ can be predicted fairly accurately from a comparison to MgO.

Table II. *Room temperature experimental critical point energies*

	$MgAl_2O_4$	α-Al_2O_3
E_0	7.8 (M_0)	8.7 (M_0)
E_1	8.9 (M_0)	9.7 (M_0)
E_2	11.0 (M_1)	11.5 (M_1)
E_3	11.9 (M_2)	11.9 (M_2)
E_4	14.0 (M_1)	12.8 (M_2)
E_5	14.7 (M_2)	14.7 (M_2)
E_6	18.9 (M_0)	17.0 (M_2)
E_7	19.5 (M_2)	

3.3. α-Al_2O_3

The measured reflectivity of (0001) oriented α-Al_2O_3 is shown in Fig. 1(c). The data displays weaker structure than the Mg-containing oxides, expected due to increased covalency. The α-Al_2O_3 reflectivity exhibits an excitonic transition at 9.1 eV followed by higher energy reflectivity peak at 32 eV associatedwith transitions from the O 2*s* state. Previous results from 8.5 to 28.5 eV show only a broad reflectivity band peaked at 13 and 20 eV with no other features resolved [3]. Shown in Fig. 2(c) is ε_2, calculated from the optical data. We resolve six critical points above the excitonic transition, as listed in Table II. We have calculated the band structure of α-Al_2O_3 [5], but the large number of atoms in the unit cell and low symmetry make simple critical point assignments difficult. We are in the process of calculating the first principles optical response using the PSF method and the detailed analysis of α-Al_2O_3 will be the subject of a future publication.

4. Exciton temperature dependence

MgO, $MgAl_2O_4$ and α-Al_2O_3 exhibit excitonic transitions associated with the Γ point band gap. These excitons have small binding energies due to the large dielectric constants, and are therefore nearly degenerate with the fundamental absorption edge. Shown in Fig. 4 are the background subtracted exciton reflectivities of MgO from room temperature

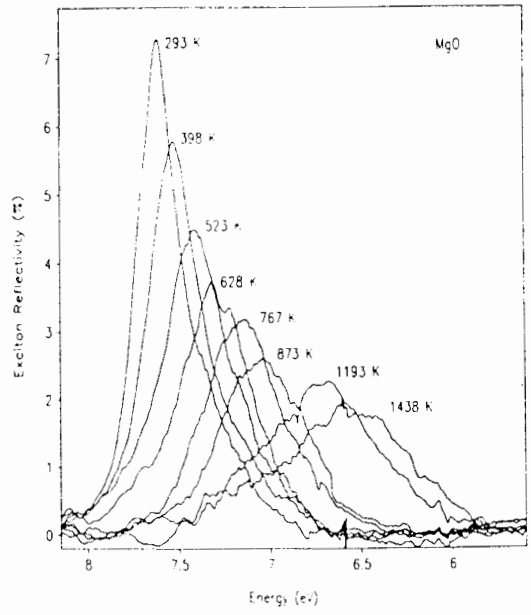

Fig. 4. Exciton reflectivity of MgO vs. temperature.

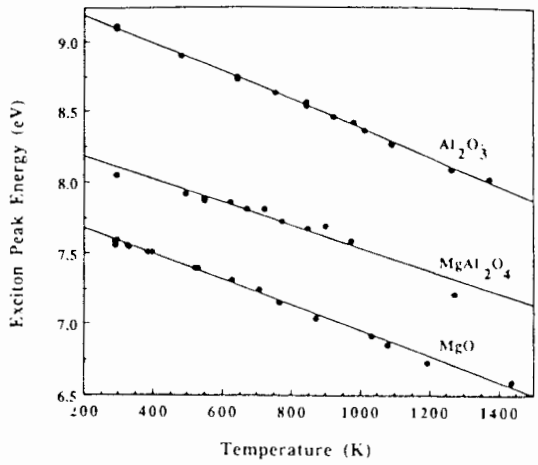

Fig. 5. Temperature dependence of the exciton peak positions of MgO, $MgAl_2O_4$ and α-Al_2O_3; temperature coefficients are -0.91, -0.78 and -1.0 meV/K respectively.

to almost 1500 K. The exciton shifts to lower energy and broadens as temperature increases. If the temperature dependence of the exciton binding energy is assumed to be small, the exciton follows the fundamental edge, giving us a simple probe of the band gap temperature dependence important for the high temperature conductivity behavior of oxide materials. Similar data was obtained for α-Al_2O_3 and $MgAl_2O_4$, and the spectra are omitted for the purposes of brevity. Shown in Fig. 5 are the exciton peak positions for the three oxides vs. temperature. The temperature coefficients vary linearly with temperature and are, -0.91, -0.78, and -1.0 meV/K for MgO, $MgAl_2O_4$, and α-Al_2O_3 respectively. These coefficients are larger than observed in the covalent semiconductors, and the same magnitude as in the alkali halides.

The exciton half width and line shape in a material are dependent on the strength of the exciton–photon coupling. The framework developed by Toyozawa predicts that weak coupling causes Lorentzian line shapes and widths that vary linearly with T, while strong coupling causes Gaussian line shapes and widths that vary as $T^{1/2}$. Shown in Fig. 6 are the temperature dependence of the exciton halfwidths of MgO and α-Al_2O_3. The MgO half width increases linearly with temperature, while the α-Al_2O_3 exciton half width increases as the square root of temperature, although scatter in the data permits a linear fit. The MgO line shape changes from Lorentzian to Gaussian near 800 K, arising from intermediate exciton-phonon coupling at 300 K with strong coupling seen at high temperature. α-Al_2O_3 and $MgAl_2O_4$ exhibit Gaussian behavior throughout the temperature range studied, suggesting that exciton–phonon coupling is stronger in more covalent oxides; however, it is important to note that defects present in the polished surfaces may effect the observed exciton-phonon coupling. $MgAl_2O_4$ crystals with high anti-site defect concentrations exhibit excitons with very wide (0.4 eV half width) gaussian line shapes, a further indication of defect induced strong coupling. Continuing measurements to low temperatures allows a determination of the effective optical phonon coupling strength [14].

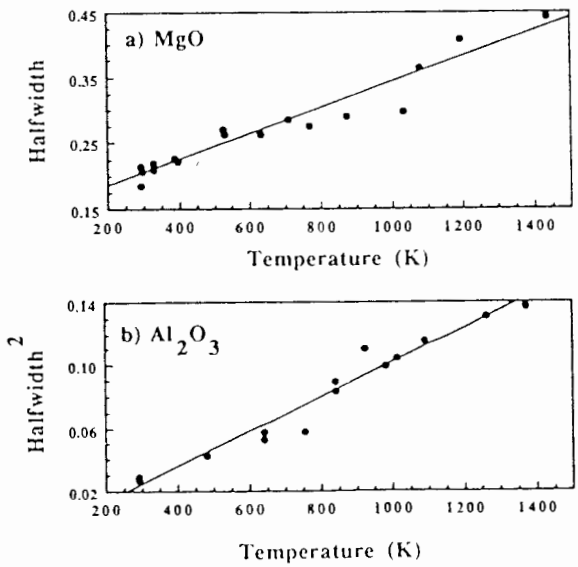

Fig. 6. Temperature dependence of the exciton halfwidths of (a) MgO and (b) α-Al_2O_3.

5. High temperature interband transitions

The sharp optical spectra of MgO make it an attractive candidate on which to perform high temperature electronic structure studies. Reducing the temperature has a minimal effect on sharpening the observed optical spectra of MgO, and the only observed change between 300 K and 77 K is a small shift and spin-orbit splitting of the exciton peak [15]. However, large changes are associated in the higher lying interband transitions at elevated temperatures. Shown in Fig. 7 are the 293 K and 1073 K ε_2 of MgO determined from the measured reflectivities. Data was also obtained at 623 K but is omitted from the figure. The difference between room temperature and 1100 K is striking, the major peaks in ε_2 all shifting to lower energy, and broadening out considerably.

Critical point analysis of the elevated temperature data allows us to determine the temperature dependence of the higher lying transitions and some of the critical points. Shown in Fig. 8 are the experimentally determined shifts in

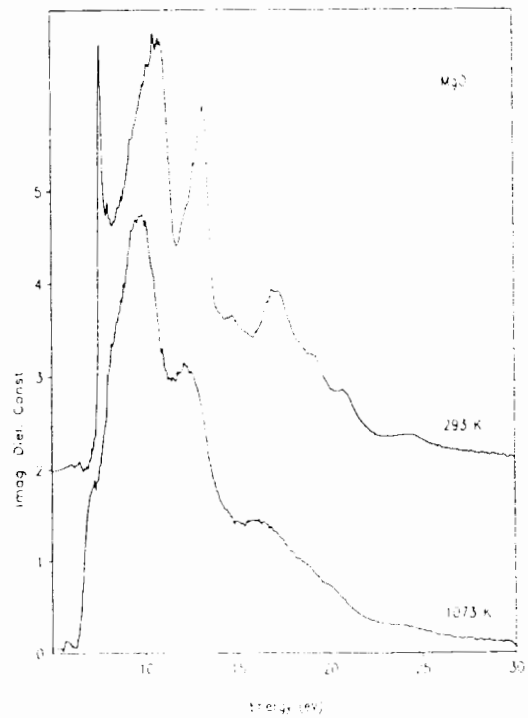

Fig. 7. ε_2 of MgO determined from the reflectivity measured at (a) 300 K and (b) 1100 K.

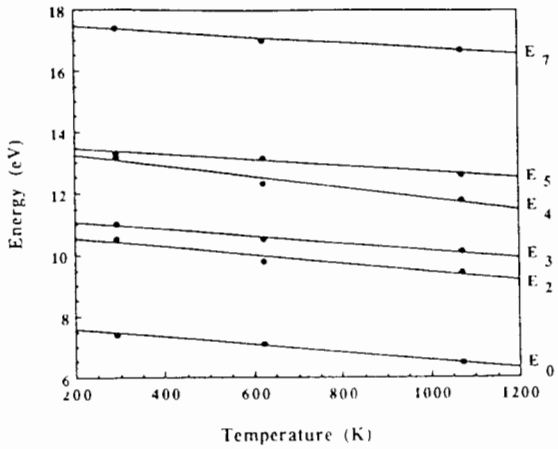

Fig. 8. Temperature dependence of the interband critical point energies of MgO. The solid lines are least squares fits to the data and the temperature coefficients in meV/K are: $E_0 = -1.22$, $E_2 = -1.30$, $E_3 = -1.12$, $E_4 = 1.71$, $E_5 = -0.92$ and $E_7 = -0.88$.

the critical points and least squares fits to the data. The data for the E_1 and E_6 transitions was insufficient to fit; we note that these are increases in ε_2 and it is easier to measure the sharp drops on the high energy side of peaks. We calculate a temperature coefficient of -1.22 meV/K for the fundamental gap, which is larger than the excitonic peak shift of -0.91 meV/K due to additional broadening. The M_1 critical point labeled E_2 decreases at -1.30 meV/K, while the M_2 point label E_3 only decreases at -1.12 meV/K. Thus we observe both the decrease and broadening of the 10.8 eV peak. The sharp peak at 14 eV broadens and shifts downward, and we measure a difference in the temperature coefficients of 0.79 meV/K between the M_1 and M_2 points which form this peak. While we could not measure the M_1 critical point labeled E_6, its companion, E_7, has the smallest measured temperature coefficient, -0.88 meV/K. It is appealing that the temperature coefficients are large at the fundmental gap and smallest for the highest interband transitions.

If we now use our assignments from Section 1 we can discuss the temperature behavior of specific band separations at certain high symmetry points in the Brillioun Zone. The separation between Γ_{15} and Γ_1 is clearly decreasing, as is the L_3–L_2' transition. Using the X_5'–X_1 assignment for the E_2 transition, we find that transitions between the top valence band and bottom conduction band have nearly the same temperature dependence at Γ and X. This is very appealing since we do not need to invoke a change in band dispersion to account for our results. Using E_5–E_2 we find that the X_4–X_5' valence band separation is increasing at 0.38 meV/K. Since the valence bands are degenerate at Γ, the lower valence band must be increasing its dispersion from Γ to X with increasing temperature. Using E_4–E_2 we find that the conduction band X_3–X_1 separation is decreasing at -0.41 meV/K. This could be the movement of the whole upper conduction band, or a change in dispersion near X.

We previously pointed out differences between our optical assignments and the previous interpretation of the MgO optical data by Roessler and Walker. Their assignments of the optical transitions combined with our measurements of the temperature dependence of the critical points lead to several conflicting results. Roessler and Walker assign the onset of the 14 eV peak in ε_2 to an M_0 transition from X_5' to X_1' and an M_1 point along Δ_5–Δ_1 near X. We measure a temperature shift of -1.71 meV/K for the M_1 point. We did not account for our optical data using an M_0 point at 12.8 eV, but the temperature shift of the valley before the peak, which is essentially the position of an M_0 point, is only -0.61 meV/K. This is a very large difference in temperature dependence if the transitions are between the same bands. Furthermore, these points are very close together in the Brillioun zone, and to account for the observed temperature behavior one must invoke large temperature dependent changes in dispersion near X. Furthermore, since the Γ point separation is decreasing at -1.22 meV/K but the X point separation at only -0.61 meV/K, dispersion changes from Γ to X are needed to account for the observed temperature behavior. Thus our assignments in MgO are more consistent with the calculated energies and the observed temperature dependence.

Acknowledgement

The authors would like to acknowledgement Milan Kokta of Union Carbide for supplying the synthetic $MgAl_2O_4$ crystal used.

References

1. Roessler, D. M. and Walker, W. C., Phys. Rev. **159**, 733 (1967).
2. Cohen, M. L., Lin, P. J., Roessler, D. M. and Walker, W. C., Phys. Rev. **155**, 992 (1966).
3. Arakawa, E. T. and Williams, M. W., J. Phys. Chem. Solids **29**, 735 (1968).
4. For example, see Lautenschlager, P., Garriga, M., Vina, L. and Cardona, M., Phys. Rev. **B36**, 4821 (1987) (and references within).
5. French, R. H., Coble, R. L., Kasowski, R. V. and Ohuchi, F. S., Physica **B150**, 47 (1988); French, R. H., J. Amer. Ceram Soc. **73**, 3 (1990).
6. French, R. H., Kasowski, R. V., Ohuchi, F. S., Jones, D. J., Song, H. and Coble, R. L., Submitted to J. Am. Cer. Soc.
7. Kasowski, R. V., Tsai, M. H., Rhodin, T. N. and Chambliss, D. D., Phys. Rev. **B34**, 2656 (1986). Kasowski, R. V., Rhodin, T. N. and Tsai, M. H., Appl. Phys. **A41**, 61 (1986). Kasowski, R. V., Rhodin, T. N. and Tsai, M. H., Appl. Phys. **A41**, 61 (1986). Kasowski, R. V., Tsai, M. H. and Rhodin, T. N., Solid State. Commun. **59**, 57 (1986).
8. Toyozawa, Y., Prog. Theor. Phys. **20**, 53 (1958).
9. Bortz, M. L. and French, R. H., Appl. Phys. Lett. **55**, 19, p. 1955 (1989).
10. French, R. H., Proceedings of the 9th Int. VUV Radiation Physics Conf., Hawaii (1989), Physica Scripta **41**, 404 (1990).
11. W. & C. Spicer Ltd. London, England, SE10 9HB.
12. Union Carbide Crystal Products Div., Washougal, WA 98671, U.S.A.
13. Bortz, M. L. and French, R. H., Applied Spectroscopy **43**, 8, p. 1498 (1989).
14. Skibowski, M., Sprussel, G. and Saile, V., Appl. Opt. **19**, 3978 (1980).
15. Roessler, R. M. and Walker, W. C., Phys. Rev. Lett. **17**, 319 (1966).